

# Hierarchical Porous Organometallic Polymers Fabricated by Direct Knitting: Recyclable Single-Site Catalysts with Enhanced Activity

Yajing Shen, Qingshu Zheng, Haibo Zhu, and Tao Tu\*

Dedicated to Prof. Li-Xin Dai on the occasion of his 95th birthday

**Porous organometallic polymers (POMPs) with hierarchical pore structures, high specific surface areas, and atomically dispersed metal (Ir, Pd, Ru) centers are successfully fabricated by a facile one-pot method through direct knitting of diverse N-heterocyclic carbene metal (NHC-M) complexes. These polymers can function as recyclable solid single-site catalysts and exhibit excellent catalytic activity and selectivity in both dehydrogenation and hydrogenation reactions even at ppm-level catalyst loadings. Remarkably, a record turnover number (TON) of  $1.01 \times 10^6$  is achieved in the hydrogenation of levulinic acid to  $\gamma$ -valerolactone, which is 750 times higher than that attained with corresponding bis-NHC-Ir complex.**

A crucial bottleneck hampering the application of immobilized molecular catalysts in industry is their reduced catalytic activity, probably due to altered chemical environment and decreased accessibility of the substrates to active sites.<sup>[1–3]</sup> Porous materials have been widely recognized as a promising scaffold for catalyst immobilization with high efficiency and reusability owing to their intrinsic porosity and high surface areas.<sup>[4–6]</sup> They can function as either heterogeneous catalysts themselves with built-in active sites or hosts with catalytic species inside their pores/channels.<sup>[7]</sup> For most metal-containing porous polymers (MCPPs),<sup>[8,9]</sup> ligands/complexes have to be carefully designed and modified,<sup>[10]</sup> which not only increase the cost and difficulty of the immobilization but may also compromise the intrinsic activity of the molecular catalysts.<sup>[11,12]</sup> To overcome these disadvantages, a facile approach for accessing

supported catalysts by simply knitting rigid aromatic ligands via hypercross-linking (Friedel-Crafts reactions) has recently been proposed.<sup>[13]</sup> After further postmodification/activation, several MCPPs have been successfully developed.<sup>[14–17]</sup> However, with postmodification, avoiding the problems, like low density of catalytic sites due to incomplete modification and random/nonselective metal anchoring, can be difficult. These issues may still lead to low catalytic activity and selectivity, especially in some challenging transformations.<sup>[18]</sup>

In light of N-heterocyclic carbene-metal (NHC-M) complexes can act as robust and viable catalysts in a broad range of reactions,<sup>[19–28]</sup> various strategies have been developed for their immobilization.<sup>[29,30]</sup> Among them, self-supporting strategy may represent one of the most practical and efficient approaches.<sup>[31–34]</sup> It has to be noted that NHC ligands still have to be carefully designed and modified before self-supporting. Alternatively, the high catalytic activities and robustness of NHC-M complexes make them perfect candidates for direct knitting. To the best of our knowledge, there are only two reported examples on MCPPs in which the NHC ligands are firstly knitted and then coordinated to active metal ions (postmodification approach).<sup>[14,15]</sup> Direct knitting of NHC-M complexes to fabricate porous organometallic polymers (POMPs) that do not require postmodification/activation is still unknown.

Herein, we have designed and prepared a series of unprecedented porous organometallic polymers POMPs-NHC-M 1–3 via direct knitting three types of bis-chelating NHC-M complexes (M = Ir, Pd, and Ru, **Figure 1a**). Using this facile strategy, which does not require postmodification/activation, 1) the metal active sites are atomically dispersed in the hierarchical porous matrix, and 2) the intrinsic well-defined bis-chelating mode and their molecular catalytic properties are maximally retained, which allows 3) the precise design and control of the immobilized catalysts at the molecular level. The advantages of direct knitting allow the resulting POMPs-NHC-M 1–3 to behave as recyclable solid single-site catalysts and exhibit extremely high catalytic activities in both hydrogenation and dehydrogenation reactions.

In light of their robustness toward Friedel-Crafts reaction conditions, bis-chelating NHC-M (Ir, Pd and Ru) complexes **4**, **5** and **6**, derived from corresponding benzimidazolium salts,<sup>[24,25,27]</sup> were selected to fabricate POMPs via direct knitting with benzene (**Figure 1a**). Concerning the plausible impact

Y. Shen, Dr. Q. Zheng, Dr. H. Zhu, Prof. T. Tu  
Shanghai Key Laboratory of Molecular Catalysis and Innovative Materials  
Department of Chemistry  
Fudan University  
2005 Songhu Road, Shanghai 200438, China  
E-mail: taotu@fudan.edu.cn

Prof. T. Tu  
State Key Laboratory of Organometallic Chemistry  
Shanghai Institute of Organic Chemistry  
Chinese Academy of Sciences  
Shanghai 200032, China

Prof. T. Tu  
College of Chemistry and Molecular Engineering  
Zhengzhou University  
100 Kexue Avenue, Zhengzhou 450001, China

 The ORCID identification number(s) for the author(s) of this article can be found under <https://doi.org/10.1002/adma.201905950>.

DOI: 10.1002/adma.201905950

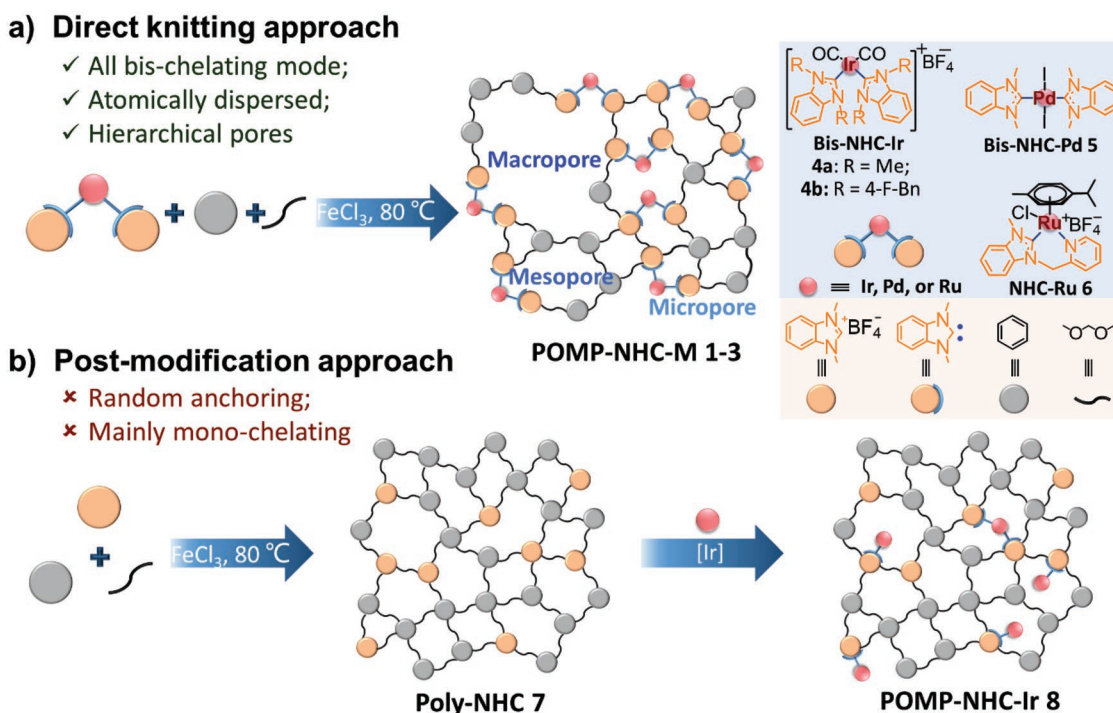


**Figure 1.** a) Fabrication of hierarchical porous organometallic polymers (POMPs-NHC-M 1–3, M: Ir, Pd, or Ru) via direct knitting of bis-NHC-M complexes 4, 5, or 6 by using Friedel-Crafts reaction in the presence of FeCl<sub>3</sub>, formaldehyde dimethyl acetal in dichloroethane with or without benzene addition. b) Fabrication of POMP-NHC-Ir 8 via postmodification of poly-NHC 7<sup>[14]</sup> with Ir(acac)(CO)<sub>2</sub>.

of the ratio between the crosslinking reagent and the Lewis acid on the porous structure, surface area and catalytic activity,<sup>[17]</sup> with bis-NHC-Ir complex 4a, the amounts of FeCl<sub>3</sub>, formaldehyde dimethyl acetal (FDA) and benzene in the knitting process were investigated for the generation of POMP-NHC-Ir 1a-h (Table 1, entries 1–8). In addition, fluorinated bis-NHC-Ir complex 4b was also involved in the direct knitting to generate corresponding POMP-NHC-Ir 1i without benzene addition (Table 1,

entry 9), which may benefit for its further characterization by using <sup>19</sup>F NMR technique. In order to verify the effect of knitting linkers, we also fabricate POMP-NHC-Ir 1j by using bis-NHC-Ir complex 4a with 1,3,5,7-tetraphenyladamantane (tAd, instead of benzene). After optimization, 20 equiv. FeCl<sub>3</sub> and 20 equiv. FDA were selected to prepare POMP-NHC-Pd 2 and POMP-NHC-Ru 3 from corresponding molecular complexes 5 and 6, respectively (Table 1, entries 10–11). For comparison,

**Table 1.** Fabrication of POMP-NHC-M by direct knitting with different ratios of FDA and FeCl<sub>3</sub>, and of POMP-NHC-Ir 8 by postmodification.

Entry <sup>a)</sup>	POMPs	Benzene [equiv.]	FeCl <sub>3</sub> [equiv.]	FDA [equiv.]	M	Metal content [%] <sup>b)</sup>	S <sub>BET</sub> [m <sup>2</sup> g <sup>-1</sup> ] <sup>c)</sup>
1	POMP-NHC-Ir 1a	3	9	9	Ir	5.69	226
2	POMP-NHC-Ir 1b	3	12	12	Ir	6.05	357
3	POMP-NHC-Ir 1c	3	15	15	Ir	6.34	440
4	POMP-NHC-Ir 1d	3	20	20	Ir	6.46	450
5	POMP-NHC-Ir 1e	1	20	20	Ir	12.9	33
6	POMP-NHC-Ir 1f	0.5	20	20	Ir	14.5	26
7	POMP-NHC-Ir 1g	0.2	20	20	Ir	14.9	24
8	POMP-NHC-Ir 1h	0	20	20	Ir	17.3	42
9	POMP-NHC-Ir 1i	0	20	20	Ir	13.3	52
10	POMP-NHC-Pd 2	3	20	20	Pd	6.97	381
11	POMP-NHC-Ru 3	3	20	20	Ru	3.93	906
12	POMP-NHC-Ir 8	3	20	20	Ir	5.37	417

<sup>a)</sup>Reaction conditions: a mixture containing 0.1 mmol of bis-chelating NHC-M complex 4a, 4b, 5, or 6, benzene, FeCl<sub>3</sub>, and FDA in 1 mL of dry dichloroethane were heated in a sealed Schlenk tube at 80 °C for 24 h under a N<sub>2</sub> atmosphere (M for Ir, Pd or Ru); <sup>b)</sup>The percentage of metal atoms were determined by ICP-AES; <sup>c)</sup>BET specific surface area calculated from the N<sub>2</sub> adsorption isotherms at 77 K.

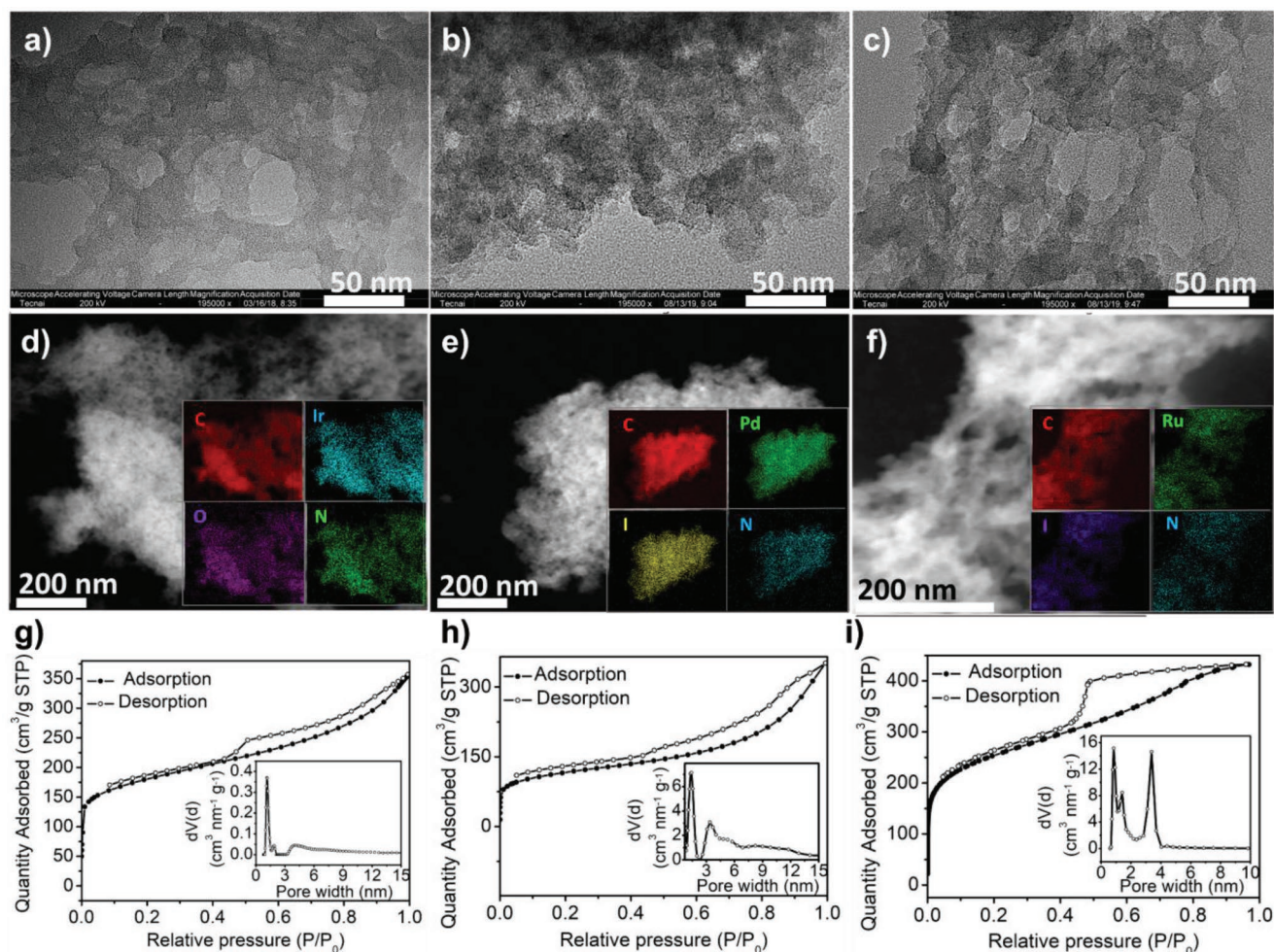


**Figure 2.** TEM and HAADF images (with EDX mapping as insets) of a,d) POMP-NHC-Ir **1d**, b,e) POMP-NHC-Pd **2**, and c,f) POMP-NHC-Ru **3**. Nitrogen adsorption and desorption isotherms of POMPs **1d**, h) **2**, and i) **3**, measured at 77 K with the corresponding pore width distribution of POMPs **1d**, **2**, and **3** determined by quenched solid density functional theory as insets.

POMP-NHC-Ir **8** was accessed via a postmodification approach from known Poly-NHC **7**<sup>[14]</sup> and Ir(acac)(CO)<sub>2</sub> (acac = acetyl acetonate, Figure 1b) as a control under the similar reaction conditions (Table 1, entry 12).

With these POMPs in hand, the morphologies were then investigated. Transmission electron microscopy (TEM) studies revealed that POMPs-NHC-Ir **1** and **8** adopted similar morphologies with porous structures (Figure 2a, and Figures S8–S11 and S17, Supporting Information). Upon increasing the amounts of FeCl<sub>3</sub> and FDA, the number of macropores increased, especially within the matrix of POMP-NHC-Ir **1d**. Similar results were also observed by scanning electron microscopy (SEM, Figures S1–S7, Supporting Information). Other POMPs based on bis-NHC-Pd **5** and NHC-Ru **6** exhibited similar lamellar morphologies with obvious macropores (Figures 2b–c). In contrast, dense lamellar morphology without obvious macropores was observed with POMP-NHC-Ir **1j** accessed by using tAd instead of benzene (Figure S18, Supporting Information). The powder X-ray diffraction (PXRD) patterns further confirmed that all obtained POMPs **1–3** and **8** were amorphous (Figure S36, Supporting Information).

The accurate metal contents of POMPs **1–3** and **8** were determined by inductively coupled plasma atomic emission spectroscopy (ICP-AES, Table 1), which clearly indicated metal contents were strongly affected by the amounts of FeCl<sub>3</sub>, FDA, and benzene as well as corresponding metal complexes. Subsequently, high-angle annular dark-field scanning transmission electron microscopy (HAADF-STEM) and energy dispersive X-ray (EDX) spectroscopy mapping indicated that metal centers were all uniformly dispersed in the matrices of all POMPs (Figure 2d–f), and no obvious iridium nanoparticles were observed even in the postmodification case (Figure S17, Supporting Information). Notably, no Fe residue was found in all solid POMPs **1–3** after Soxhlet extraction and repeated rinse with water and methanol, further confirmed by EDX and X-ray photoelectron spectroscopy (XPS) analysis (Figures S24 and S38, Supporting Information). To our surprise, Cl element was found in the EDX and XPS spectra with low intensity, which may be attributed to the partial ligand exchange of weak coordinated CO ligands with the Cl elements presented in the chlorinated solvent DCE and FeCl<sub>3</sub> during the knitting process.<sup>[35]</sup>

The porosities of the POMPs 1–3 and 8 were then investigated by nitrogen sorption measurements. The adsorption and desorption isotherms of POMP-NHC-Ir **1d** show steep increases in the  $N_2$  uptake in the  $P/P_0 < 0.05$  region, which is a typical behavior of microporous materials (Figure 2g). The capillary condensation hysteresis between  $P/P_0$  0.45 and 1.00 indicates also the presence of mesopores. Further analysis of the pore size distribution using quenched solid density functional theory (QSDFT)<sup>[36]</sup> reveals a dominant pore width at 0.9–1.5 nm, a small peak at 1.6–2.1 nm and a broad peak at 3.0–8.0 nm (Figure 2g). Similar porosities were observed with POMPs 1a–c (Table 1, entries 1–3, Figure S25a,b, Supporting Information). Therefore, combining with the macropores observed in TEM images (Figure 2a), POMP-NHC-Ir **1d** actually possesses hierarchical pores, including micropores, mesopores, and macropores with the highest Brunauer–Emmett–Teller (BET) specific surface areas ( $450 \text{ m}^2 \text{ g}^{-1}$ , Table 1, entry 4) in all fabricated POMPs, suggesting the higher amount of FDA and  $\text{FeCl}_3$ , the larger the BET and the portion of micropores. Other POMPs 2 and 3 also showed hierarchical porous structures (Table 1, entries 10–11, Figure 2h,i), further indicated the generality of our direct knitting strategy. Decreasing the equivalents of benzene had great impact on the  $N_2$  sorption properties, not only much lower BET specific surface areas were obtained, but also the pore structures were different, the percentage of mesopores and macropores were significantly enhanced (Table 1, entries 5–8, Figures S27–S30, Supporting

Information). Extremely, in the case of POMP NHC-Ir **1j** formed with tAd, mainly micropores along with a little content of mesopores were observed (Figure S35, Supporting Information). Surprisingly, the BET specific surface areas of Poly-NHC **7**, fabricated under the standard knitting conditions with **1d**, was very high ( $1068 \text{ m}^2 \text{ g}^{-1}$ , Figure S34, Supporting Information). However, after postmodification with iridium species, the specific surface area of POMP-NHC-Ir **8** was drastically decreased to  $417 \text{ m}^2 \text{ g}^{-1}$ , which might be caused by the occupation of iridium species to the existed pores within the POMP matrices.

The successful immobilization of bis-chelating NHC-M complexes within the polymer matrices was further confirmed by Fourier transform infrared (FT-IR) spectroscopy, solid-state  $^{13}\text{C}$  NMR spectroscopy and XPS (Figure 3a,b and Figure S45, Supporting Information). In the case of POMP-NHC-Ir **1d**, the presence of the absorption band at  $2088 \text{ cm}^{-1}$  in its FT-IR spectra, corresponding to the CO ligand attached to the iridium center,<sup>[25]</sup> indicated the successful knitting of bis-NHC-Ir complex **4a** (Figure S45, Supporting Information). In the solid-state  $^{13}\text{C}$  NMR spectra (Figure 3a, blue line, Figure S50, Supporting Information), peaks for  $C_{\text{Ar}}$  (135 ppm, aromatic rings) and  $C_{\text{Me}}$  (35 ppm, N-methyl groups and bridging methylene) in the POMPs correspond well with those observed in bis-NHC-Ir **4a**. However, the broad signals for  $C_{\text{NHC}}$  and  $C_{\text{CO}}$  ( $\approx 190$  ppm) are uncertainly assigned, even with more than 100 mg samples, due to the extremely low NHC content (0.8 % based on Ir) in the

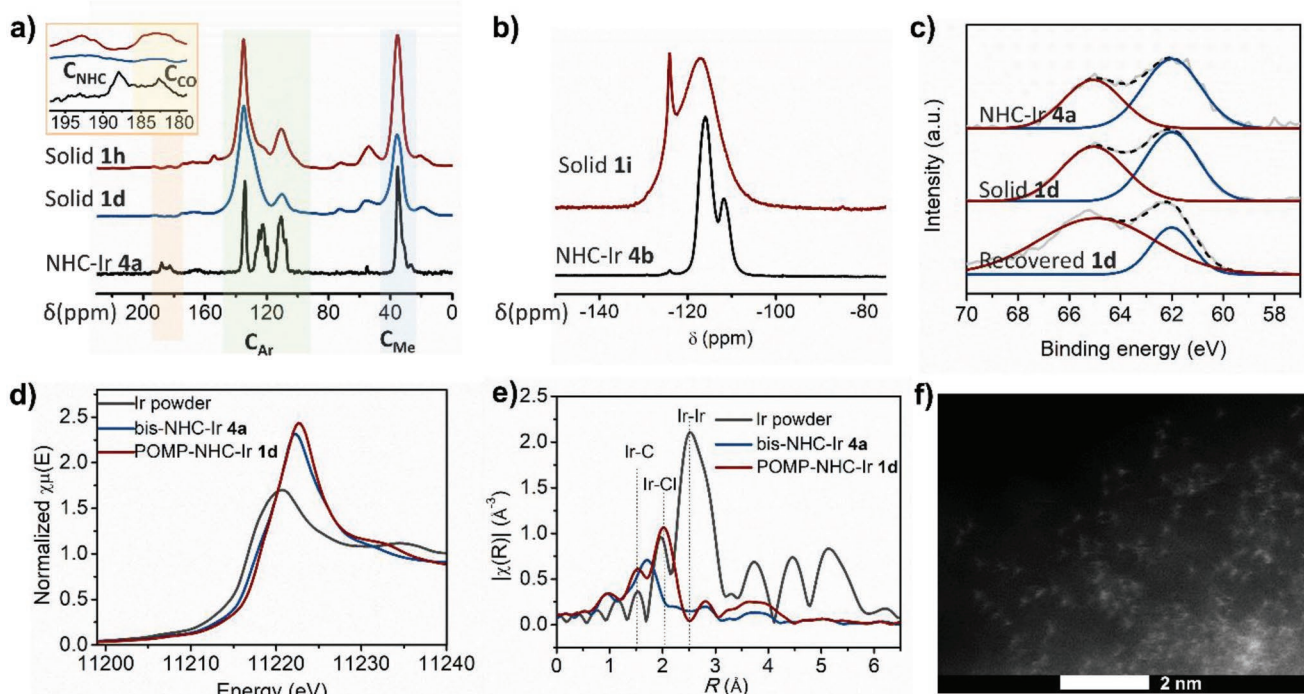


**Figure 3.** a) Solid-state  $^{13}\text{C}$  NMR spectra of POMP-NHC-Ir **1h** (red line), **1d** (blue line), and bis-NHC-Ir **4a** (black line). Note: asterisks denote spinning sidebands.<sup>[14,15,44]</sup> b) Solid-state  $^{19}\text{F}$  NMR spectra of POMP-NHC-Ir **1i** (red line) and bis-NHC-Ir **4b** (black line). c) X-ray photoelectron spectroscopy (XPS) spectra of Ir(II) in molecular complex **4a**, freshly prepared solid **1d**, and recovered **1d** from the reaction mixture after 15 runs of the hydrogenation of LA to GVL. d) Normalized XANES spectra at the  $L_3$  edge of solid **1d**, the standard Ir(0) powder, and NHC-Ir(I) complex **4a** were added for comparison. e) Magnitude of Fourier transformed Ir L-edge EXAFS spectra of solid **1d** and references. All the spectra were determined via least-squares EXAFS curve fitting analysis. f) Magnified HAADF-STEM images of solid **1d**, the well dispersed white dots represented iridium atoms.

POMP matrix of solid **4a**.<sup>[37]</sup> To solve this ambiguous problem, POMP-NHC-Ir **1h** fabricated via direct knitting with molecular precursor **4a** without benzene addition was also investigated by solid-state <sup>13</sup>C NMR spectroscopy. Fortunately, signals for C<sub>NHC</sub> and C<sub>CO</sub> (193 and 183 ppm) were distinguishable with 200 mg solid samples loading, although the intensity was still low (Figure 3a). The similar chemical shifts of C<sub>NHC</sub> observed with solids **1h** and **4a** (193 vs 188 ppm) indicate the complex structure should be well preserved after direct knitting. To make this conclusion more convincing, fluorinated POMP-NHC-Ir **1i**, obtained from fluoro-containing bis-NHC-Ir complex **4b** after knitting, was analyzed by both solid-state <sup>13</sup>C NMR and <sup>19</sup>F NMR. Broad but almost identical signals were observed in the <sup>19</sup>F NMR spectra with solid samples of POMP-NHC-Ir **1i** and complex **4b** (Figures 3b and Figure S51, Supporting Information), further emphasizing the structure preservation of the robust bis-NHC-Ir complex during direct knitting. Besides, the thermostability of solid **1d** was studied by thermogravimetric analysis (TGA). The decomposition temperature is relatively high (300 °C, Figure S37, Supporting Information), confirming its robustness.

Furthermore, to our delight, almost identical binding energies of 65.0 eV (Ir 4f<sub>5/2</sub>) and 62.0 eV (Ir 4f<sub>7/2</sub>) for POMP-NHC-Ir **1d** and bis-NHC-Ir **4a** were found in the XPS spectra (Figure 3c), indicating that the oxidation state of the Ir(I) in POMP-NHC-Ir **1d** was well retained after direct knitting. Similar results were obtained with the POMP-NHC-Pd **2** and POMP-NHC-Ru **3**. The binding energies of Pd(II) in POMP-NHC-Pd **2** were 342.9 eV (3d<sub>3/2</sub>) and 337.7 eV (3d<sub>5/2</sub>), which were quite close to the 342.8 eV (3d<sub>3/2</sub>) and 337.6 eV (3d<sub>5/2</sub>) in bis-NHC-Pd complex **5**, indicating the Pd maintained the oxidation state of +2 after direct knitting (Figure S42, Supporting Information). In the case of POMP-NHC-Ru **3**, only 3d<sub>5/2</sub> signal was selected to study the coordination environment of Ru in the POMP matrix owing to the spectra interference with the 1s signal of C. As shown in Figure S41 (Supporting Information), identical binding energy was observed with POMP-NHC-Ru **3** and NHC-Ru complex **6**, further confirmed the oxidation state of Ru center in the POMP matrix was +2. In contrast, signals at 65.6 eV (4f<sub>5/2</sub>) and 62.6 eV (4f<sub>7/2</sub>) were observed in the post-modification case, which suggested the coexistence of mono-NHC-Ir and bis-NHC-Ir species in the matrix of POMP-NHC-Ir **8** (Figures S39 and S40, Supporting Information). All these outcomes clearly indicated the well-defined molecular structures of NHC-M (+1, +2) complexes were well preserved in the POMP 1–3 matrices fabricated by direct knitting strategy.

Subsequently, the chemical oxidation state and coordination environment of iridium in the matrix of POMP-NHC-Ir **1d** were further investigated by X-ray absorption near-edge structure (XANES) and extended X-ray absorption fine structure (EXAFS) analyses. The normalized Ir-L<sub>3</sub> edge in the XANES spectra of solid **1d**, standard iridium powder and structurally defined bis-NHC-Ir **4a** are shown in Figure 3d. The XANES curve of solid **1d** is quite similar to that of molecular complex **4a**. The intensity of the Ir-L<sub>3</sub> white line increased along the sequence Ir powder < bis-NHC-Ir **4a** ≈ solid **1d**. Based on the results of Ir(0) in iridium powder, Ir(I) in complex **4a**, the stable valence state of the Ir centers in the **1d** matrix should be ≈ +1, which is consistent with the XPS results (Figure 3c).

To obtain the quantitative structural parameters involving the single iridium atoms, least-squares EXAFS curve fitting analysis was performed. The Fourier transform of the k<sup>2</sup>-weighted EXAFS fitted curves were consistent with the experimental results (Figure S54, Supporting Information). The absence of Ir–Ir bonds in POMP-NHC-Ir **1d** (Figure 3e, Table S1, Supporting Information) implied that the Ir(I) centers are atomically well dispersed in the polymer matrix. Considering that chlorine was found in XPS and EDS studies (Figures S24 and S38, Supporting Information) due to partial exchange of CO ligands with Cl elements of chlorinated solvent and FeCl<sub>3</sub> during the knitting process,<sup>[37]</sup> Ir–Cl bond was implemented for EXAFS data fitting. The obtained good R-factor of 0.012 suggested the existence of Ir–Cl bond with small quantity within the polymer matrix. Furthermore, the Ir–C interaction at 2.03 Å with a coordination number of 4.1 observed with solid **1d** is smaller than that at 2.08 Å with a coordination number of 5.6 found with complex bis-NHC-Ir **4a** (Figure 3e).<sup>[38]</sup> Despite the slight change of coordination environment around Ir center, the bis-chelating backbone of complex **4a** were well preserved. Remarkably, magnified HAADF-STEM images showed well dispersed white dots, indicating that individual Ir atoms were atomically dispersed in the matrix of solid **1d**. Similarly, the atomically dispersed Pd and Ru dots can also be found in the corresponding HAADF-STEM images (Figures S14 and S16, Supporting Information). These outcomes clearly indicated that POMP with single-site metal atoms were readily achieved via direct knitting.

In the case of postmodification, the XANES curve of POMP-NHC-Ir **8** displayed a higher intensity of the Ir-L<sub>3</sub> white line than that observed with solid **1d** and complex **4a** (Figure S55a, Supporting Information), which was consistent with the XPS results. The EXAFS spectra also revealed the absence of Ir–Ir bonds in the solid **8**, and the Ir–C interaction at 2.08 Å with a coordination number of 10.0, which was greater than that observed with molecular complex **4a** (2.08 Å, coordination number of 5.6, Figure S55b, Supporting Information), which might confirm the coexistence of mono-NHC-Ir and bis-NHC-Ir species in the matrix of POMP-NHC-Ir **8**.

Having these POMP with hierarchical porosity and atomically dispersed active sites in hand, their activities function as single-site catalysts<sup>[39–43]</sup> were then investigated. As an important platform molecule in laboratory and industrial applications, γ-valerolactone (GVL) has attracted considerable attention.<sup>[31,45–50]</sup> Therefore, the hydrogenation of biomass levulinic acid (LA) to GVL was selected as the first model reaction. After careful catalyst screening and optimization of the reaction conditions (Table S2, Supporting Information), a quantitative yield was finally achieved in the presence of 130 ppm POMP-NHC-Ir **1d** under 30 atm hydrogen at 100 °C within 4 h. Other POMP 1a–c all resulted in lower yields (49–88%, Figure 4a), which might be ascribed to the lesser content of active Ir(I) and the smaller BET surfaces areas (Table 1, entries 1–3 and 12 vs 4). Therefore, the amounts of FeCl<sub>3</sub> and FDA used for the direct knitting not only affect the morphologies, but also exhibit obvious impacts on their catalytic activities: higher amount of FeCl<sub>3</sub> and FDA, higher yields. As a comparison, the POMP-NHC-Ir **8** prepared via postmodification using the same amounts of FeCl<sub>3</sub> and FDA for solid **1d** fabrication, only gave a yield of 68%. The existence of less-active mono-coordination

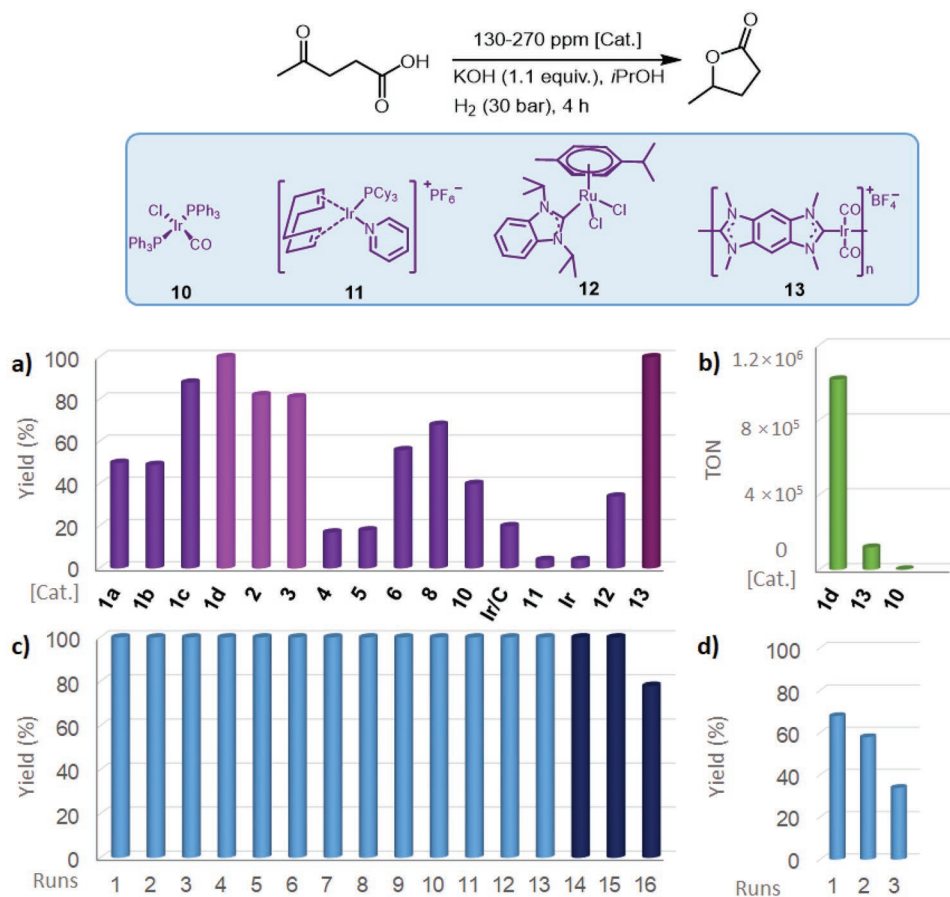


**Figure 4.** a) Catalyst optimization in the hydrogenation of LA to GVL. Reaction condition: 15 mmol Levulinic acid, 1.1 equiv. KOH and 5 mL *i*PrOH were added into the autoclave, then 130 ppm catalysts were added and the reaction mixture was reacted under 30 bar H<sub>2</sub> pressure at 100 °C for 4 h. Yield was determined by <sup>1</sup>H NMR. b) Turnover numbers (TONs) obtained by POMP and other selected viable catalysts. Reusability of c) POMP-NHC-Ir **1d** and d) POMP-NHC-Ir **8** (carried out on a 15 mmol scale with 270 ppm catalyst under the optimized reaction conditions) for 4 h (light blue) or for 24 h (dark blue).

NHC-Ir motif as well as the entrapped inactive iridium species in the matrix pores of POMP-NHC-Ir **8** might be responsible for this disappointed outcome.

Compared with the homogenous analogues, including complexes bis-NHC-Ir **4a**, bis-NHC-Pd **5**, and NHC-Ru **6**, POMP-NHC-Ir **1d**, POMP-NHC-Pd **2**, and POMP-NHC-Ru **3** exhibited much higher catalytic activities under otherwise identical reaction conditions (17% vs 99%, 18% vs 82%, and 56% vs 81%, Figure 4a). It has to be pointed out, there are few reports on Pd-catalyzed hydrogenation of LA to GVL under hydrogen atmosphere,<sup>[51,52]</sup> and good result and enhanced catalytic activity could be achieved by POMP-NHC-Pd **2** even at 130 ppm catalyst loadings. Furthermore, other privileged and commercially available catalysts (**10-12**)<sup>[46-50]</sup> were also employed in this transformation, only trace to inferior yields were obtained under optimal reaction conditions (Figure 4a). Although our previously reported self-supported catalyst **13** also gave a quantitative yield under the identical reaction conditions,<sup>[31]</sup> a record turnover number (TON) of  $1.01 \times 10^6$  could be achieved by further decreasing the catalyst loading of POMP-NHC-Ir **1d** to 0.678 ppm (Figure 4b). This TON value is one order of magnitude higher than that of self-supported catalyst

**13** ( $1.2 \times 10^5$ ),<sup>[31]</sup> and at least three orders of magnitude higher than those achieved by previously reported Ir, Ru, Zr, and Cu inorganic nanoparticles (up to  $8.2 \times 10^3$ , Table S4, Supporting Information).

After the hydrogenation reaction, solid **1d** was readily recovered by simple centrifugation, filtration, and wash with additional MeOH. To our delight, the recovered solid **1d** can be directly reused in the second run of reaction simply by recharging the vessel with LA, KOH, and *i*-PrOH, and no significant loss in the yield of GVL was observed. At 270 ppm catalyst loading, solid **1d** could be reused for 13 runs under the optimized reaction conditions (4 h, Figure 4c, light blue). By slightly extending the reaction time to 24 h, quantitative yields could still be achieved for two more runs (Figure 4c, dark blue). Additionally, the reusability of POMP-NHC-Ir **8** was also carried out under the otherwise identical reaction conditions. Poor yield was found even at the first run, and continuously declined yields were observed in the subsequent cycles, probably due to random anchoring and existence of mono-NHC-Ir species in the solid matrix of **8** (Figure 4d).

The properties of solids **1d** and **8** during the hydrogenation process were characterized by ICP-AES, TEM, XPS, and FT-IR.

ICP-AES revealed that after the first run with solid **1d**, negligible iridium leaching occurred in subsequent runs (Table S5, Supporting Information). The metal leaching (1.6% of the original Ir content in solid **1d**) observed in the first run could be attributed to decomposed iridium species that were trapped in the pores of the matrix during the knitting process. TEM images revealed that the freshly prepared and recovered **1d** had similar morphologies (Figure 1a vs Figure S19, Supporting Information). And XPS analysis gave almost identical peaks for the fresh and recovered **1d** (Figure 3c). These results clearly demonstrate that no iridium agglomeration or cluster formation occurred during recycle of the solid **1d**, and thus the polymer matrix is helpful for avoiding dimerization and aggregation which are often observed in homogenous bis-NHC-Ir complexes.<sup>[53–56]</sup> In contrast, high iridium leaching was observed with solid **8** accessed by postmodification (9.4% lost after three runs, Table S6, Supporting Information), and Ir(0) species were observed in the recovered solid **8**, confirmed by XPS analysis (Figure S43, Supporting Information). Further TEM study confirmed the formation of iridium nanoparticles during the hydrogenation reaction catalyzed by solid **8** (Figure S21, Supporting Information).

Noticeably, an absorption band at 2088 cm<sup>-1</sup> (attributed to CO ligands) was not visible in the FT-IR spectrum of recovered solid **1d** (Figure S45 in the Supporting Information, blue line vs red line). This result implied that CO ligands were weakly coordinated to the Ir center and might dissociate during the reaction process. To confirm this assumption, a control experiment was performed in which CO was bubbled through a suspension of recovered solid **1d**, and this process was conducted according to a literature procedure for preparation of homogeneous bis-NHC-Ir(CO)<sub>2</sub> complexes.<sup>[25]</sup> To our delight, the CO signal reappeared after CO bubbling (Figure S45, black line, Supporting Information), confirming that CO was weakly bound to the Ir(I) center. This observation revealed that POMPs may behave like homogeneous molecular catalysts, allowing precise design and control of immobilized catalysts at the molecular level. And the slight alternation of coordination environment around the Ir center in the solid **1d** did not affect its catalytic activity, as supported by the unchanged high catalytic efficiency during the catalyst recycling experiments (Figure 4c).

To further probe why the performance of POMPs **1d**, **2** and **3** exhibited much higher catalytic activity than the corresponding molecular complexes **4–6**, several control experiments were carried out. In the case of bis-NHC-Pd(II) **5** and NHC-Ru(II) **6**, Pd and Ru nanoparticles were found in the TEM images after reactions (Figures S22 and S23, Supporting Information) and also could be successfully isolated by centrifugation. Mercury drop test<sup>[57]</sup> (Table S3, Supporting Information) with no obvious decrease in yield suggested the metal nanoparticles formed during the process hardly catalyzed reaction. Hence, the inferior yields obtained by complexes **5** and **6** might be attributed to the formation of inactive metal nanoparticles during the hydrogenation. However, when two drops of Hg were also added into the reaction mixture with bis-NHC-Ir **4a** as catalyst, neither decrease in yield nor iridium nanoparticles were found. Taking account of the possible dimer formation with bis-NHC-Ir complexes,<sup>[53–56]</sup> POMPs-NHC-Ir **1h–i** by direct knitting of complexes **4a–b** without benzene addition

were also involved. Compared with their molecular precursors, higher catalytic activities were observed with the corresponding POMPs (17% vs 99%, and 4% vs 60%, respectively, Table S2, entries 12–13, Supporting Information). In this context, we believed the formation of iridium dimer species with molecular bis-NHC-Ir complex **4a** in the LA to GVL transformations was the only reason leading to the lower activity. In addition, when the POMP-NHC-Ir **1j** with mainly micropores was employed in the hydrogenation of LA to GVL under standard reaction conditions, a decreased yield (87%) was obtained, suggesting macropores may indeed accelerate the mass and heat transfer to increase the transformation efficiency (Table S2, entry 21, Supporting Information).

With all these control experiments, the ultrahigh activity of solid **1d** can be mainly attributed to i) isolation effect endowed by the linkers within the matrix, which efficiently prevented the formation of possible inactive dimers, oligomers, or nanoparticles from bis-NHC-Ir motifs during the reactions; ii) the structurally preserved bis-chelating modes and atomically dispersed metal centers with similar retained chemical environment to its molecular catalyst; and iii) its unique hierarchical porosity, in which the micropores potentially enhanced its catalytic activity due to pore confinement effects,<sup>[7]</sup> and the mesopores and the macropores allowed rapid mass and heat transfer.<sup>[58]</sup> All of these issues are critical and helpful for the reaction activity improvements with POMPs.

Because bis-NHC-Ir complexes can serve as bifunctional catalysts in various transformations,<sup>[25,26]</sup> after investigation of their applicability in the hydrogenation reaction, we further explored the bifunctional catalytic applicability of solid **1d** in oxidative reactions. Considering the increasing global demand for lactic acid, which is a raw material in the syntheses of biodegradable polylactide materials, pharmaceuticals, foods and green solvents,<sup>[59]</sup> its synthesis via the dehydrogenation of glycerol, a main waste product of the biodiesel and soap industries,<sup>[60]</sup> was selected as a model reaction. As expected, solid **1d** exhibited excellent activity and selectivity (99%) in this challenging transformation even at 340 ppm catalyst loading (Table S7, Supporting Information). In contrast, POMP-NHC-Ir **8**, prepared by the postmodification approach, hardly accelerated the transformation, and almost no product was detected under otherwise identical reaction conditions, further highlighting the advantage of the direct knitting approach. Solid **1d** could also be reused for six times. After the sixth run, over 90% yield was still achieved (Figure S56, Supporting Information). ICP-AES analysis indicated that > 99% of the Ir(I) species were still immobilized in the solid polymer matrix after six runs at 115 °C for 36 h (Table S8, Supporting Information). Similar TEM morphologies, XPS images and FT-IR spectra were observed for the freshly prepared and recovered solid **1d** (Figures S20, S44, and S46). All these results clearly demonstrated that solid **1d** could function as a highly efficient, bifunctional, single-site solid catalyst.

In summary, we have successfully fabricated a series of robust porous organometallic polymers (POMPs) with hierarchical pore structures, high specific surface areas and atomically dispersed metal sites (Ir, Pd, and Ru) via a direct knitting approach. The intrinsic properties of the active and structure-defined bis-chelating NHC-metal complexes with different

valence states (+1 to +2) are highly preserved during immobilization, enabling these solid POMPs function as single-site bifunctional catalysts with excellent activity and selectivity in both dehydrogenation and hydrogenation reactions. Remarkably, a record turnover number (TON:  $1.01 \times 10^6$ ) was achieved in the hydrogenation of levulinic acid to  $\gamma$ -valerolactone, and the POMP-NHC-Ir could be reused for up to 15 runs without obvious losses of catalytic activity or selectivity even at ppm-level catalyst loadings. This study demonstrates not only that hierarchical porous single-site solid catalysts can be readily fabricated by direct knitting of privileged organometallics but also that these immobilized catalysts can be precisely designed and controlled at the molecular level. All these outcomes may pave the way for direct accessing and tuning recyclable heterogeneous catalysts based on privileged homogeneous catalysts while maintaining or even enhancing the catalytic activities. Following work of extending the direct knitting approach to other privileged homogeneous catalysts, such as metalloporphyrins and metal-pincer complexes, are ongoing in our laboratory.

## Experimental Section

**Synthesis of POMPs-NHC-M 1–3:** In the case of POMP-NHC-Ir **1d**, bis-NHC-Ir complex **4a**<sup>[25]</sup> (0.1 mmol, 63 mg) and benzene (or 0.3 mmol, 23 mg) were dissolved in 1 mL of dry anaerobic 1,2-dichloroethane (DCE) under N<sub>2</sub> atmosphere. After stirring, anhydrous FeCl<sub>3</sub> (2.0 mmol, 324 mg) and formaldehyde dimethyl acetal (FDA, 2.0 mmol, 152 mg) were added. The resulting mixture was heated to 80 °C and stirred for 24 h under a nitrogen atmosphere. After cooling to room temperature, the precipitate was collected and washed by methanol, distilled water, dichloromethane, and acetone successively. Further purification of the polymer was carried out by Soxhlet extraction from methanol for 48 h. The product was dried in vacuum for 24 h at 60 °C to give a dark brown powder (Yield: 90%). The preparation of POMPs-NHC-Ir **1a–c** and **1e–g** was similar to that of POMP-NHC-Ir **1d**, except the amount of FeCl<sub>3</sub>, FDA and benzene were varied (see the Supporting Information). In the case of solids **1h** and **1i**, bis-NHC-Ir complexes **4a** and **4b** were directly knitted without benzene. The POMP **1j** was prepared by using similar procedure to that of POMP-NHC-Ir **1d**, except that 1,3,5,7-tetraphenyladamantane was used instead of benzene. Following the same synthetic procedure of solid **1d**, POMPs-NHC-Pd **2** and NHC-Ru **3** were readily obtained from molecular complexes bis-NHC-Pd(II) **5** and NHC-Ru(II) **6**, respectively. In addition, after tableting the resulted POMPs powder into sheet, the conductivity of these polymer materials was also investigated by multimeter and four-point probe method, no obvious conductivity was found.

## Supporting Information

Supporting Information is available from the Wiley Online Library or from the author.

## Acknowledgements

Financial support from the Ministry of Science and Technology of China (No. 2016YFA0202902), the National Natural Science Foundation of China (Nos. 21861132002, 21871059, and 21572036), and the Department of Chemistry, Fudan University is gratefully acknowledged. The authors also thank Prof. Yongning Zhou, Dr. Jiong Li, and the BL14W1 at the Shanghai Synchrotron Radiation Facility for XAS experiment.

## Conflict of Interest

The authors declare no conflict of interest.

## Keywords

biomass transformation, direct knitting, N-heterocyclic carbene metal complexes, porous organometallic polymers, single-site catalysts

Received: September 11, 2019

Revised: November 13, 2019

Published online:

- [1] Z. Wang, G. Chen, K. Ding, *Chem. Rev.* **2009**, *109*, 322.
- [2] *Handbook of Asymmetric Heterogeneous Catalysis* (Eds: K. Ding, Y. Uozumi), Wiley-VCH, Weinheim **2008**.
- [3] J. A. Gladysz, *Chem. Rev.* **2002**, *102*, 3215.
- [4] A. G. Slater, A. I. Cooper, *Science* **2015**, *348*, aaa8075.
- [5] J. Liu, N. P. Wickramaratne, S. Z. Qiao, M. Jaroniec, *Nat. Mater.* **2015**, *14*, 763.
- [6] J. Wu, F. Xu, S. Li, P. Ma, X. Zhang, Q. Liu, R. Fu, D. Wu, *Adv. Mater.* **2019**, *31*, 1802922.
- [7] Q. Sun, Z. Dai, X. Meng, F.-S. Xiao, *Chem. Soc. Rev.* **2015**, *44*, 6018.
- [8] G. Li, S. Zhao, Y. Zhang, Z. Tang, *Adv. Mater.* **2018**, *30*, 1800702.
- [9] S. Kramer, N. R. Bennedsen, S. Kegnæs, *ACS Catal.* **2018**, *8*, 6961.
- [10] D. Zhao, D. J. Timmons, D. Yuan, H.-C. Zhou, *Acc. Chem. Res.* **2011**, *44*, 123.
- [11] W. Wang, A. Zheng, P. Zhao, C. Xia, F. Li, *ACS Catal.* **2014**, *4*, 321.
- [12] Z. Xie, C. Wang, K. E. deKrafft, W. Lin, *J. Am. Chem. Soc.* **2011**, *133*, 2056.
- [13] L. Tan, B. Tan, *Chem. Soc. Rev.* **2017**, *46*, 3322.
- [14] S. Xu, K. Song, T. Li, B. Tan, *J. Mater. Chem. A* **2015**, *3*, 1272.
- [15] Z. Jia, K. Wang, T. Li, B. Tan, Y. Gu, *Catal. Sci. Technol.* **2016**, *6*, 4345.
- [16] B. Li, Z. Guan, W. Wang, X. Yang, J. Hu, B. Tan, T. Li, *Adv. Mater.* **2012**, *24*, 3390.
- [17] B. Li, R. Gong, W. Wang, X. Huang, W. Zhang, H. Li, C. Hu, B. Tan, *Macromolecules* **2011**, *44*, 2410.
- [18] Y. Zhang, S. N. Riduan, *Chem. Soc. Rev.* **2012**, *41*, 2083.
- [19] A. Doddi, M. Peters, M. Tamm, *Chem. Rev.* **2019**, *119*, 6994.
- [20] C. Fliedel, A. Labande, E. Manoury, R. Poli, *Coord. Chem. Rev.* **2019**, *394*, 65.
- [21] D. A. Hey, R. M. Reich, W. Baratta, F. E. Kühn, *Coord. Chem. Rev.* **2018**, *374*, 114.
- [22] S. Shi, S. P. Nolan, M. Szostak, *Acc. Chem. Res.* **2018**, *51*, 2589.
- [23] D. Janssen-Müller, C. Schleppehorst, F. Glorius, *Chem. Soc. Rev.* **2017**, *46*, 4845.
- [24] S. Movassaghi, S. Singh, A. Mansur, K. K. H. Tong, M. Hanif, H. U. Holtkamp, T. Söhnle, S. M. F. Jamieson, C. G. Hartinger, *Organometallics* **2018**, *37*, 1575.
- [25] M. G. Manas, J. Campos, L. S. Sharninghausen, E. Lin, R. H. Crabtree, *Green Chem.* **2015**, *17*, 594.
- [26] J. Campos, U. Hintermair, T. P. Brewster, M. K. Takase, R. H. Crabtree, *ACS Catal.* **2014**, *4*, 973.
- [27] G. M. Roberts, P. J. Pierce, L. K. Woo, *Organometallics* **2013**, *32*, 2033.
- [28] C. F. Rentzsch, E. Tosh, W. A. Herrmann, F. E. Kühn, *Green Chem.* **2009**, *11*, 1610.
- [29] R. Zhong, A. C. Lindhorst, F. J. Groche, F. E. Kühn, *Chem. Rev.* **2017**, *117*, 1970.
- [30] W. Wang, L. Cui, P. Sun, L. Shi, C. Yue, F. Li, *Chem. Rev.* **2018**, *118*, 9843.
- [31] Y. Liu, Z. Sun, C. Huang, T. Tu, *Chem. - Asian J.* **2017**, *12*, 355.

- [32] Z. Sun, J. Chen, T. Tu, *Green Chem.* **2017**, *19*, 789.
- [33] Z. Sun, Y. Liu, J. Chen, C. Huang, T. Tu, *ACS Catal.* **2015**, *5*, 6573.
- [34] S. M. Sarker, Y. Uozumi, Y. M. Yamada, *Angew. Chem.* **2011**, *123*, 9609; *Angew. Chem., Int. Ed.* **2011**, *50*, 9437.
- [35] K. H. G. Mak, P. K. Chan, W. Y. Fan, W. K. Leong, Y. Li, *J. Organomet. Chem.* **2013**, *741-742*, 176.
- [36] A. V. Neimark, Y. Lin, P. I. Ravikovitch, M. Thommes, *Carbon* **2009**, *47*, 1617.
- [37] M. Rodriguez-Castillo, G. Lugo-Preciado, D. Laurencin, F. Tielens, A. van der Lee, S. Clement, Y. Guari, J. M. Lopez-de-Luzuriaga, M. Monge, F. Remacle, S. Richeter, *Chem. - Eur. J.* **2016**, *22*, 10446.
- [38] B. J. van Weerdenburg, A. H. Engwerda, N. Eshuis, A. Longo, D. Banerjee, M. Tessari, C. F. Guerra, F. P. Rutjes, F. M. Bickelhaupt, M. C. Feiters, *Chem. - Eur. J.* **2015**, *21*, 10482.
- [39] X. Su, X. F. Yang, Y. Huang, B. Liu, T. Zhang, *Acc. Chem. Res.* **2019**, *52*, 656.
- [40] S. Wei, A. Li, J. C. Liu, Z. Li, W. Chen, Y. Gong, Q. Zhang, W. C. Cheong, Y. Wang, L. Zheng, H. Xiao, C. Chen, D. Wang, Q. Peng, L. Gu, X. Han, J. Li, Y. Li, *Nat. Nanotechnol.* **2018**, *13*, 856.
- [41] A. Han, W. Chen, S. Zhang, M. Zhang, Y. Han, J. Zhang, S. Ji, L. Zheng, Y. Wang, L. Gu, C. Chen, Q. Peng, D. Wang, Y. Li, *Adv. Mater.* **2018**, *30*, 1706508.
- [42] P. Liu, Y. Zhao, R. Qin, S. Mo, G. Chen, L. Gu, D. M. Chevrier, P. Zhang, Q. Guo, D. Zang, B. Wu, G. Fu, N. Zheng, *Science* **2016**, *352*, 797.
- [43] X.-F. Yang, A. Wang, B. Qiao, J. Li, J. Liu, T. Zhang, *Acc. Chem. Res.* **2013**, *46*, 1740.
- [44] P.-F. Wei, M.-Z. Qi, Z.-P. Wang, S.-Y. Ding, W. Yu, Q. Liu, L.-K. Wang, H.-Z. Wang, W.-K. An, W. Wang, *J. Am. Chem. Soc.* **2018**, *140*, 4623.
- [45] W. Cao, L. Lin, H. Qi, Q. He, Z. Wu, A. Wang, W. Luo, T. Zhang, *J. Catal.* **2019**, *373*, 161.
- [46] X. Zhang, P. Zhang, C. Chen, J. Zhang, G. Yang, L. Zheng, J. Zhang, B. Han, *Green Chem.* **2019**, *21*, 54.
- [47] S. Li, Y. Wang, Y. Yang, B. Chen, J. Tai, H. Liu, B. Han, *Green Chem.* **2019**, *21*, 770.
- [48] D. M. Alonso, S. G. Wettstein, J. A. Dumesic, *Green Chem.* **2013**, *15*, 584.
- [49] J. Q. Bond, D. M. Alonso, D. Wang, R. M. West, J. A. Dumesic, *Science* **2010**, *327*, 1110.
- [50] L. Deng, J. Li, D. M. Lai, Y. Fu, Q. X. Guo, *Angew. Chem.* **2009**, *121*, 6651; *Angew. Chem., Int. Ed.* **2009**, *48*, 6529.
- [51] B. Banerjee, R. Singuru, S. K. Kundu, K. Dhanalaxmi, L. Bai, Y. Zhao, B. M. Reddy, A. Bhaumik, J. Mondal, *Catal. Sci. Technol.* **2016**, *6*, 5102.
- [52] C. Michel, J. Zaffran, A. M. Ruppert, J. Matras-Michalska, M. Jedrzejczyk, J. Grams, P. Sautet, *Chem. Commun.* **2014**, *50*, 12450.
- [53] J. Campos, L. S. Sharninghausen, R. H. Crabtree, D. Balcells, *Angew. Chem., Int. Ed.* **2014**, *53*, 12808; *Angew. Chem.* **2014**, *126*, 13022.
- [54] L. S. Sharninghausen, J. Campos, M. G. Manas, R. H. Crabtree, *Nat. Commun.* **2014**, *5*, 5084.
- [55] S. P. Smidt, A. Pfaltz, E. Martínez-Viviente, P. S. Pregosin, A. Albinati, *Organometallics* **2003**, *22*, 1000.
- [56] R. Crabtree, *Acc. Chem. Res.* **1979**, *12*, 331.
- [57] K. Yu, W. Sommer, J. M. Richardson, M. Weck, C. W. Jones, *Adv. Synth. Catal.* **2005**, *347*, 161.
- [58] B. Fang, J. H. Kim, M.-S. Kim, J.-S. Yu, *Acc. Chem. Res.* **2013**, *46*, 1397.
- [59] M. Dusselier, P. Van Wouwe, A. Dewaele, E. Makshina, B. F. Sels, *Energy Environ. Sci.* **2013**, *6*, 1415.
- [60] M. R. Monteiro, C. L. Kugelmeier, R. S. Pinheiro, M. O. Batalhad, A. da Silva Césare, *Renewable Sustainable Energy Rev.* **2018**, *88*, 109.